A retractable lid in lecithin:cholesterol acyltransferase provides a structural mechanism for activation by apolipoprotein A-I

Kelly A. Manthei[1], Joomi Ahn[2], Alisa Glukhova[1,3], Wenmin Yuan[4], Christopher Larkin[2], Taylor D. Manett[1], Louise Chang[1], James A. Shayman[5], Milton J. Axley[2], Anna Schwendeman[4], John J.G. Tesmer[1†]

[1] From the Life Sciences Institute and the Departments of Pharmacology and Biological Chemistry, University of Michigan, Ann Arbor, Michigan 48109
[2] MedImmune, Gaithersburg, MD 20878
[3] Current address: Drug Discovery Biology, Monash Institute of Pharmaceutical Sciences Biology, and Department of Pharmacology, Monash University, Parkville, Victoria 3052, Australia
[4] Department of Pharmaceutical Science, Biointerfaces Institute, University of Michigan, Ann Arbor, MI
[5] Department of Internal Medicine, University of Michigan, Ann Arbor, Michigan 48109

Running title: *The closed lid conformation of LCAT*

Table of Contents

Table S1. pNPB hydrolysis and ΔT_m of LCAT variants.

Variant	Location	ΔT_m ± SD (°C)	n	Esterase rate ± SD (A_{400}/min)	n
WT			18	0.014 ± 0.003	39
ΔNΔC		1.2 ± 1	4	0.025 ± 0.004	5
S181A	Active site	-0.67 ± 0.3	3	0.0059 ± 0.001	3
W48A	MBD	3.1 ± 1	3	0.024 ± 0.001	3
L70S	MBD	0.53 ± 0.3	3	0.028 ± 0.002	3
T123A	ApoA-I?	-0.40 ± 0.4	3	0.014 ± 0.003	4
T123I[a]	ApoA-I?	1.2 ± 0.2	3	0.016 ± 0.001	4
N131A	ApoA-I?	-0.73 ± 0.3	3	0.014 ± 0.002	3
N131D[a]	ApoA-I?	-2.1 ± 1	4	0.0074 ± 0.001	3
F382A	ApoA-I?	0.17 ± 0.5	6	0.034 ± 0.006	8
F382V[a]	ApoA-I?	0.24 ± 0.6	5	0.012 ± 0.002	5
F382E	ApoA-I?	-0.80 ± 0.26	3	0.026 ± 0.002	3
N391A	ApoA-I?	-2.0 ± 0.7	4	0.011 ± 0.002	3
N391S[a]	ApoA-I?	-1.4 ± 0.4	3	0.0094 ± 0.001	3
G230R[a]	Lid	-1.0 ± 0.3	3	0.023 ± 0.002	4
P232A	Lid	-0.87 ± 0.5	3	0.017 ± 0.002	4
I233A	Lid	-0.63 ± 0.3	3	0.026 ± 0.0009	3
I233E	Lid	-2.3 ± 0.3	3	0.025 ± 0.002	3
M234A	Lid	-0.57 ± 0.5	3	0.019 ± 0.002	3
S235A	Lid	-0.73 ± 0.3	3	0.016 ± 0.001	4
S236A	Lid	0.20 ± 0.6	3	0.018 ± 0.001	3
Δlid	Lid	1.3 ± 1	11	0.028 ± 0.008	8
Δlid/F382A	Lid/ApoA-I?	1.8 ± 0.6	3	0.032 ± 0.003	4
LPLA2lid	Lid	-2.0 ± 0.5	3	0.013 ± 0.002	3
LPLA2αA	αA-αA′ loop	-1.3 ± 0.4	3	0.011 ± 0.001	3

[a]indicates disease-related mutants

MBD indicates membrane-binding domain; ApoA-I? indicates disease-related surface-exposed residues that could potentially bind ApoA-I

Table S2. LCAT binding to ApoA-I and peptide HDLs measured by BLI.

Variant	ApoA-I HDLs			22A HDLs		
	Response ± SD (nm)	**% of WT ± SD**	**n**	**Response ± SD (nm)**	**% of WT ± SD**	**n**
WT	0.18 ± 0.02		16	0.28 ± 0.03		14
ΔNΔC	0.023 ± 0.01	14 ± 8	2	0.025 ± 0.002	11 ± 0.3	2
S181A	0.10 ± 0.006	61 ± 0.4	2	0.17 ± 0.02	68 ± 10	2
W48A	0.029 ± 0.008	17 ± 5	2	0.041 ± 0.007	15 ± 5	3
L70S	0.027 ± 0.004	16 ± 3	2	0.021 ± 0.005	7.7 ± 3	3
T123A	0.17 ± 0.007	89 ± 5	2	0.25 ± 0.02	90 ± 6	2
T123I	0.14 ± 0.02	73 ± 7	2	0.20 ± 0.008	72 ± 6	2
N131A	0.15 ± 0.0	80 ± 5	2	0.20 ± 0.02	74 ± 20	2
N131D	0.082 ± 0.01	45 ± 9	2	0.13 ± 0.01	43 ± 4	2
F382A	0.27 ± 0.1	120 ± 30	6	0.29 ± 0.03	100 ± 20	4
F382V	0.19 ± 0.01	96 ± 10	2	0.29 ± 0.002	100 ± 5	2
F382E	0.21 ± 0.02	110 ± 10	2	0.31 ± 0.02	110 ± 5	2
N391A	0.12 ± 0.007	63 ± 5	2	0.17 ± 0.01	61 ± 8	2
N391S	0.12 ± 0.01	63 ± 8	2	0.19 ± 0.01	67 ± 7	2
G230R	0.078 ± 0.006	42 ± 2	2	0.14 ± 0.02	46 ± 8	2
P232A	0.081 ± 0.005	44 ± 0	2	0.142 ± 0.00	48 ± 1	2
I233A	0.041 ± 0.004	21 ± 3	2	0.083 ± 0.01	29 ± 4	2
I233E	0.048 ± 0.001	26 ± 2	2	0.056 ± 0.006	20 ± 2	2
M234A	0.079 ± 0.001	43 ± 4	2	0.14 ± 0.002	48 ± 3	2
S235A	0.16 ± 0.02	95 ± 10	4	0.26 ± 0.004	88 ± 0.5	2
S236A	0.062 ± 0.03	36 ± 20	4	0.20 ± 0.03	67 ± 10	2
Δlid	0.073 ± 0.01	40 ± 9	7	0.078 ± 0.02	29 ± 8	6
Δlid/F382A	0.089 ± 0.003	48 ± 4	2	0.10 ± 0.001	34 ± 1	2
LPLA2lid	0.061 ± 0.005	35 ± 3	4	0.090 ± 0.006	33 ± 9	3
LPLA2αA	0.057 ± 0.009	29 ± 1	2	0.042 ± 0.003	15 ± 2	3

Table S3. LCAT acyltransferase activity with ApoA-I HDLs.

Variant	V_{max} ± SD (μM/hr)	K_m ± SD (μM)	V_{max}/K_m	Sig.[b]	n
WT	14 ± 0.3	11 ± 0.6	1.3		22
ΔNΔC	ND[a]	ND		**	3
S181A	ND	ND		**	3
W48A	17 ± 0.7	21 ± 2	0.81	ns	3
L70S	15 ± 0.7	19 ± 2	0.79	ns	3
T123A	0.79 ± 0.4	1.9 ± 5	0.42	**	3
T123I	1.5 ± 0.5	ND		*	3
F382A	0.27 ± 0.2	ND		**	6
F382V	2.2 ± 0.4	0.96 ± 1.4	2.3	*	3
F382E	0.51 ± 0.6	ND		**	3
N131A	20 ± 1	12 ± 2	1.7	ns	3
N131D	2.8 ± 0.4	3.6 ± 2	0.78	*	3
N391A	5.3 ± 0.4	3.5 ± 1	1.5	ns	3
N391S	5.0 ± 0.4	2.6 ± 0.9	1.9	ns	3
G230R	7.9 ± 0.5	3.7 ± 1	2.1	ns	3
P232A	7.1 ± 0.4	4.7 ± 1	1.5	ns	3
I233A	11 ± 0.6	11 ± 2	1.0	ns	3
I233E	ND	ND		**	3
M234A	12 ± 0.7	6.2 ± 1	1.9	ns	3
S235A	7.6 ± 0.5	5.2 ± 1	1.5	ns	3
S236A	11 ± 1	4.8 ± 2	2.3	ns	3
Δlid	0.52 ± 0.2	ND		**	8
Δlid/F382A	0.48 ± 0.2	ND		**	3
LPLA2 lid	2.4 ± 0.3	0.65 ± 0.8	3.7	*	3
LPLA2 αA	0.40 ± 0.3	ND		**	3

[a]ND = not determined, signal too low to determine an accurate fit
[b]Sig. represents significance compared to WT using a two-tailed t-test, ns indicates not significant, *0.01<P<0.05, **0.001<P<0.01

Figure S1

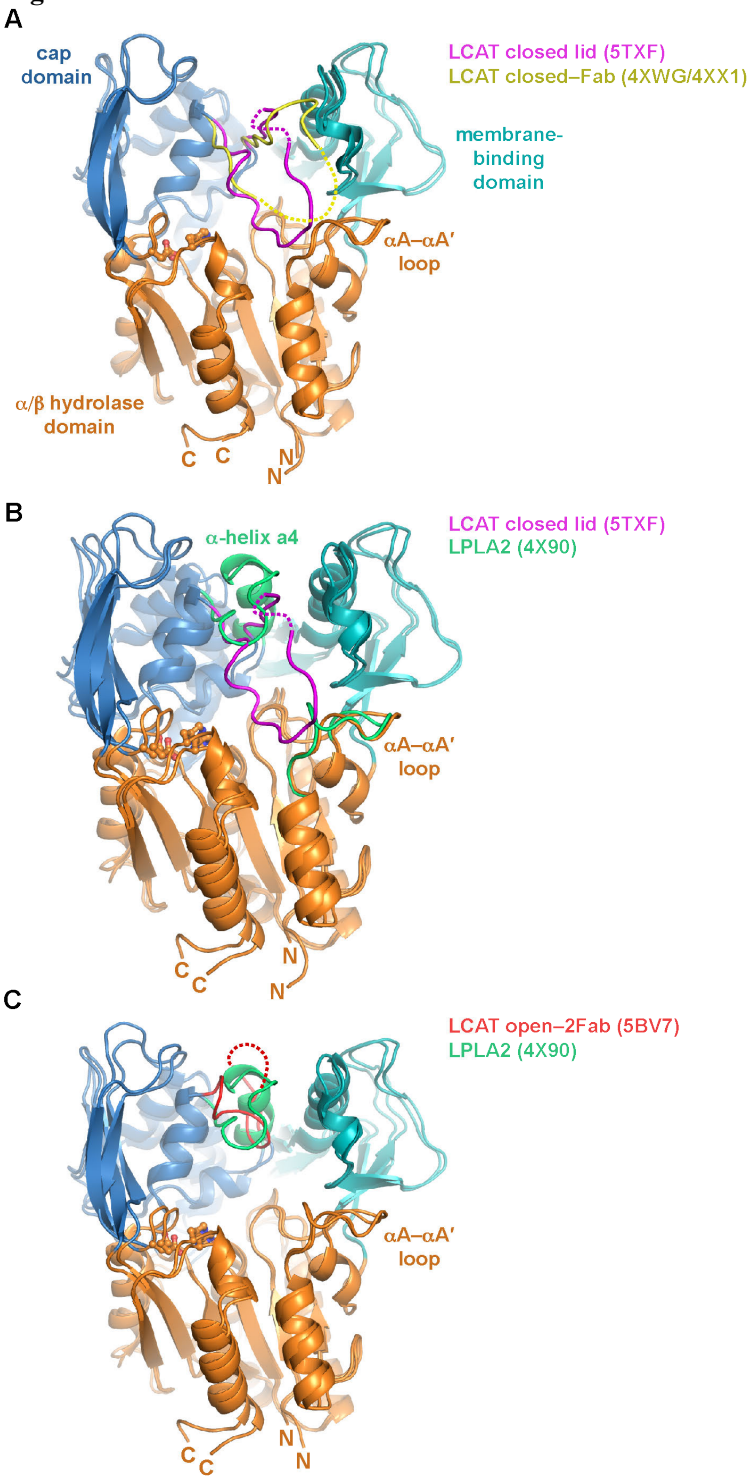

Figure S1. Comparison of different open and closed LCAT and LPLA2 structures. (*A*) Closed LCAT structure described here (PDB entry 5TXF) overlaid with closed–Fab (4XWG, contains mutation C31Y). (*B*) LCAT superimposed with LPLA2 (4X90) with large structural differences shown in green. Notably, the lid is retracted and the αA-αA′ loop is two residues longer in LPLA2, which would clash with the lid conformation observed in the closed structure of LCAT. (*C*) Open–2Fab structure (5BV7) overlaid with LPLA2. Unmodeled residues are indicated with dashed lines.

Figure S2

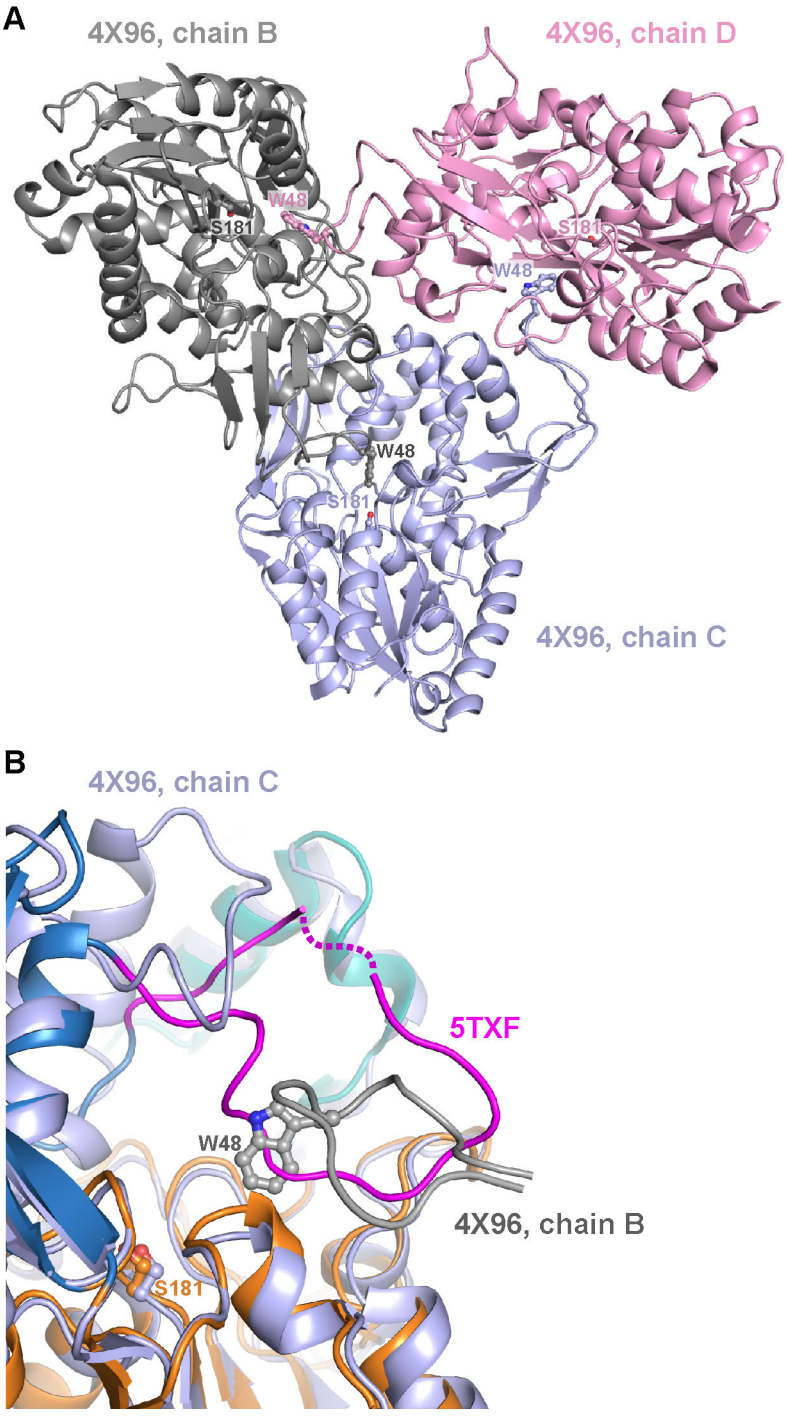

Figure S2. Low-resolution LCAT structure must adopt an open conformation due to crystal packing interactions. (**a**) In the low-resolution structure (4X96), LCAT crystallized as a trimer with Trp48 (shown as ball-and-sticks) docked in the active site (represented by Ser181) of another LCAT protomer. (**b**) The closed structure reported here (5TXF) is overlaid with 4X96 to show that the extended lid is incompatible with the low-resolution structure crystal packing.

Figure S3

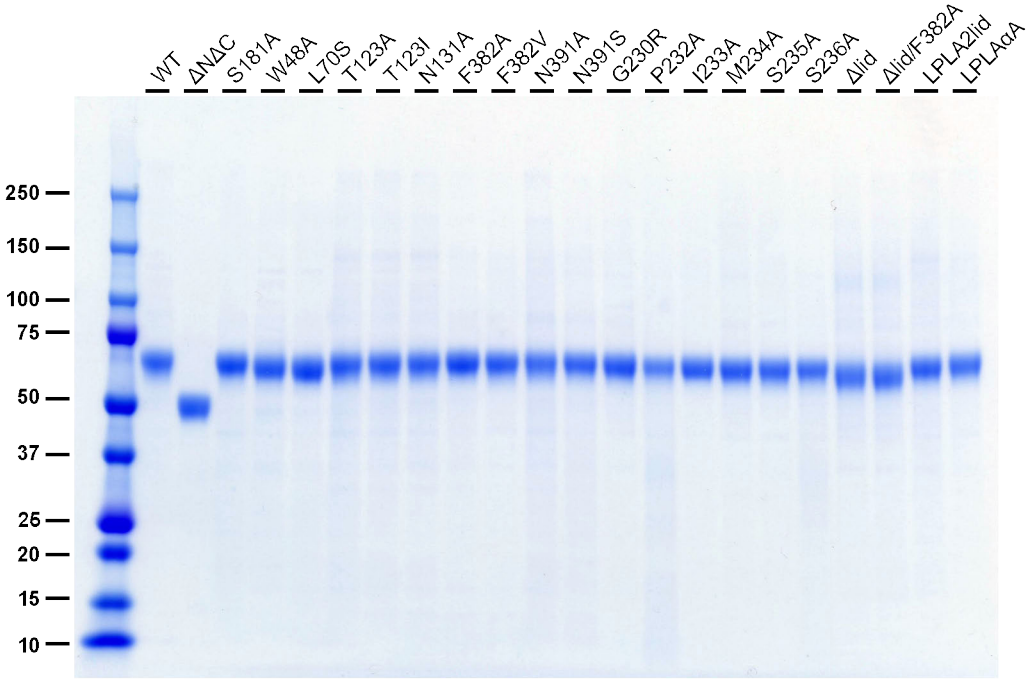

Figure S3. Gel of purified LCAT variants. Approximately 1.5 µg of each purified LCAT variant used in biochemical analysis was loaded to the gel. Variants N131D, F382E, and I233E are not shown in this gel, but were of comparable purity.

Figure S4

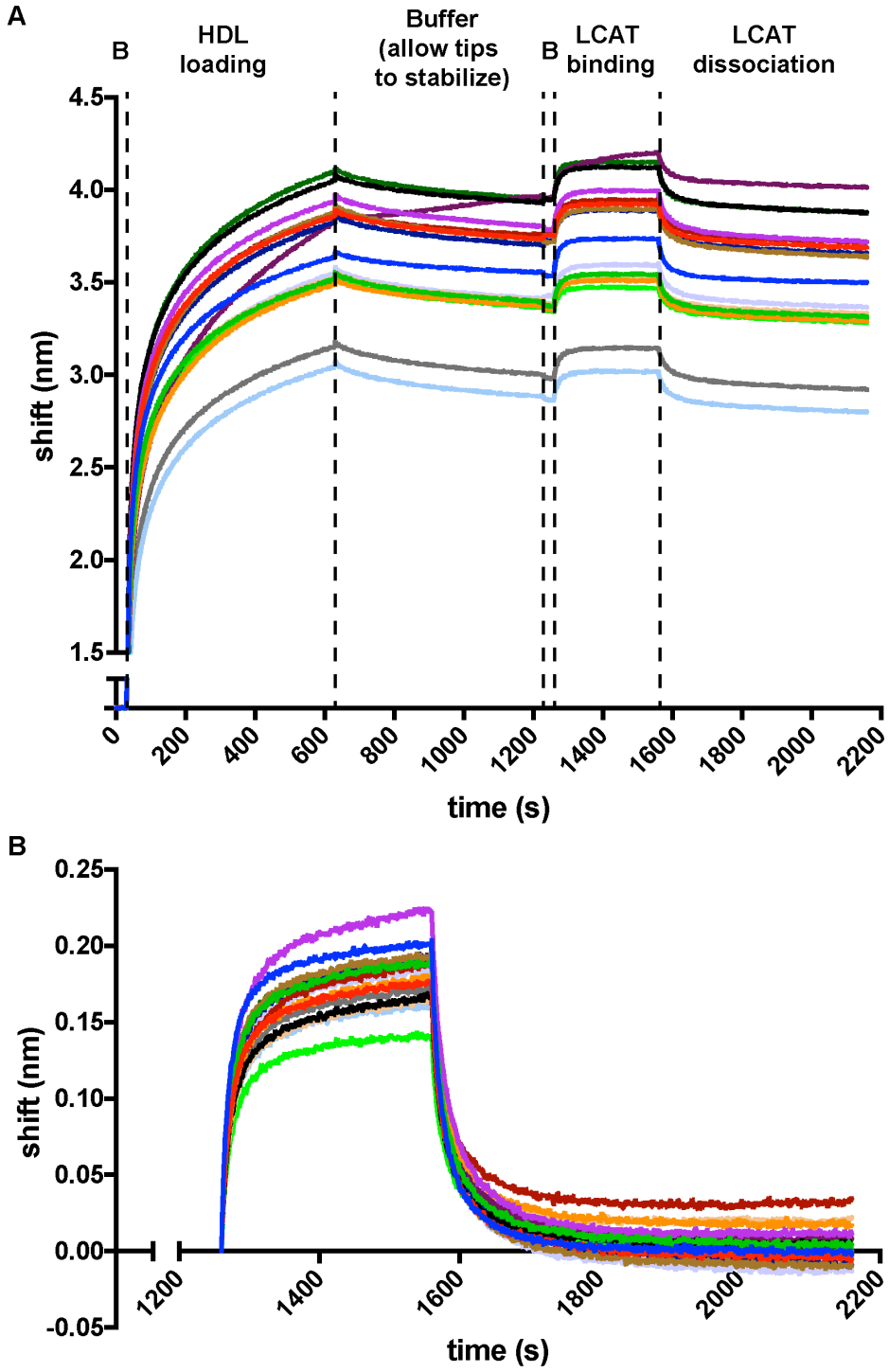

Figure S4. Comparison of BLI loading data. (*A*) 16 different replicates of WT LCAT binding to ApoA-I HDLs are shown to compare HDL loading. In all 16 the ApoA-I HDL sample was diluted 1/20 and 0.2 μM LCAT was used in the binding step. B refers to a 30 s baseline step. (*B*) The LCAT binding and dissociation steps are shown after buffer and baseline subtraction to show that the different levels of HDL loading do not correlate with the final magnitude of LCAT binding. The color of the curve indicates the same experiment in each panel.

Figure S5

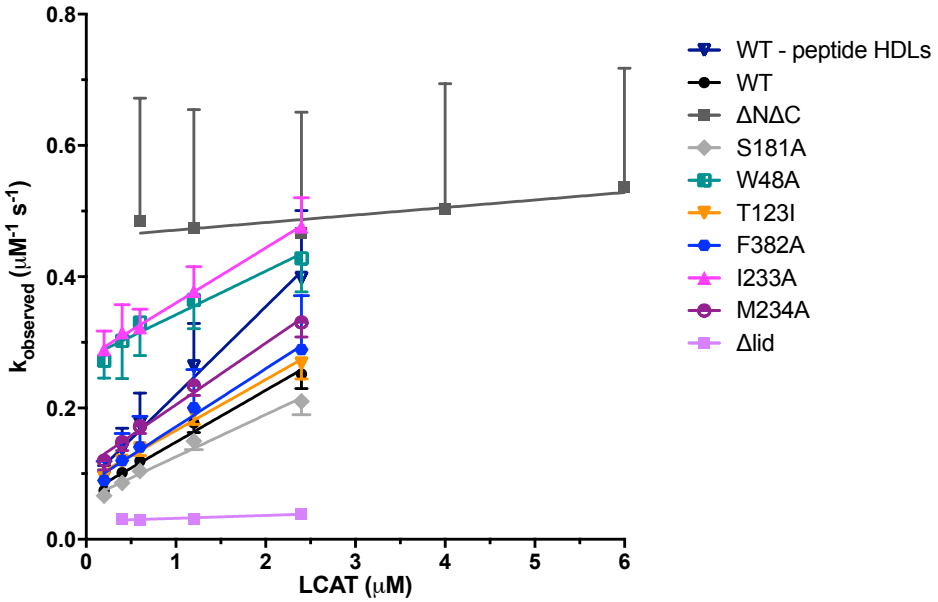

Figure S5. Plots used to determine k_{on} (slope of fit line) and hence K_d (see methods). All measurements were taken with ApoA-I HDLs except for WT LCAT with peptide HDLs, as indicated.

Figure S6

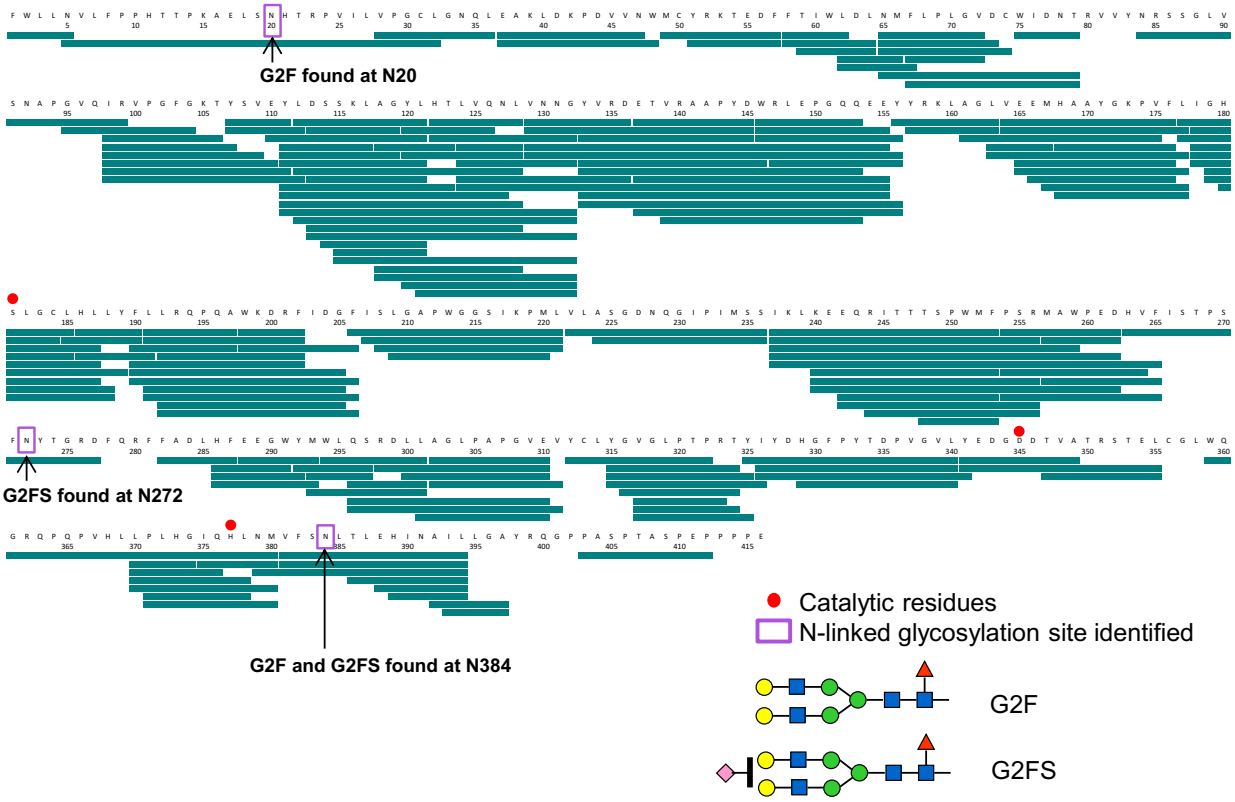

Figure S6. 95% of LCAT sequence coverage achieved by online pepsin digestion. Reproducible peptide fragments (shown as green bars) were produced in both IDFP bound and unbound forms. A total of 187 peptides were reproducibly generated in all 50 digestions. N-linked glycosylation was observed, as expected, at Asn20, Asn272, and Asn384, however N-linked glycosylation at Asn84 and O-linked glycosylation at Thr407 and Ser409 were not observed.

Figure S7

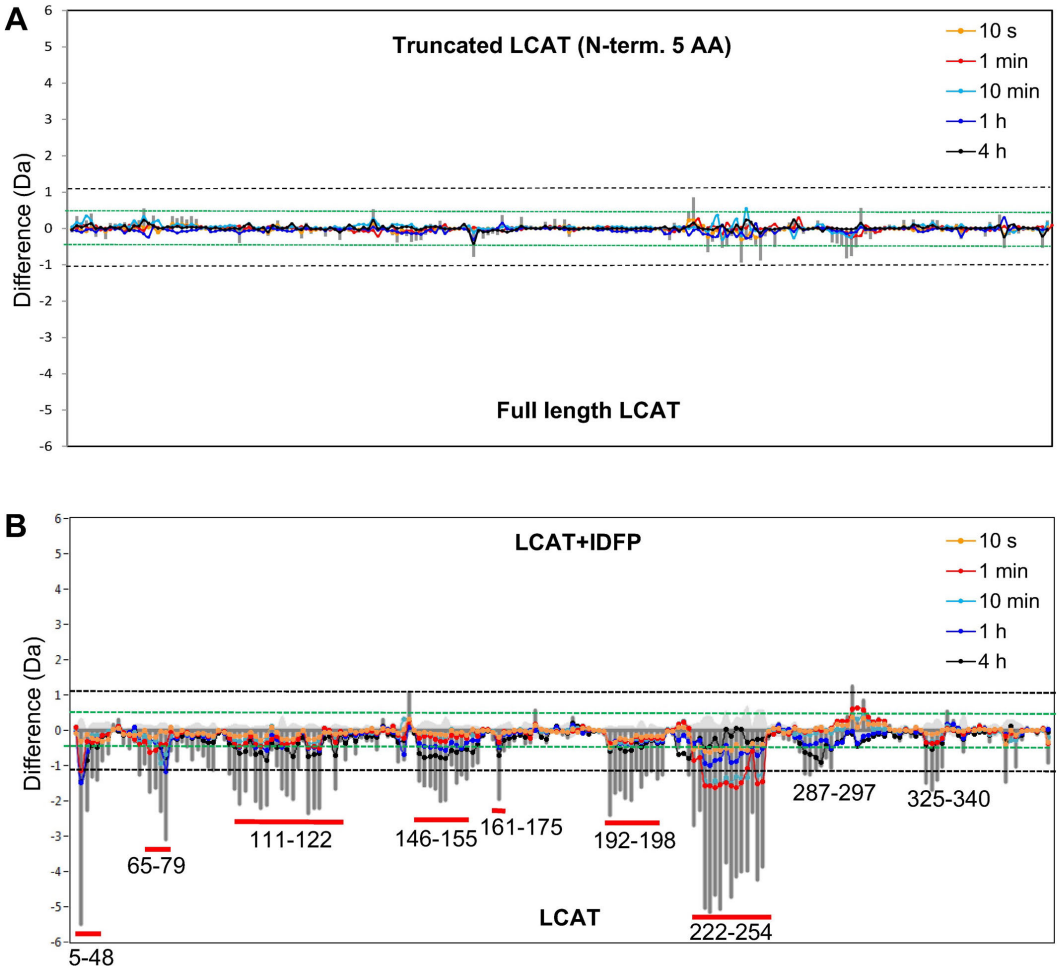

Figure S7. HDX MS difference plots. (*A*) The difference plot is the difference (y-axis) of deuterium uptake (Da) between truncated LCAT (top) and full length LCAT (bottom). Overall measured exchange for all peptides were not significantly different for any of the time-points. The green dotted lines at y-axis values +0.5 Da represent the 98% confident limits for difference between individual time points, whereas the black dotted lines at y-axis +1.1 Da indicate the boundary of significance for the sum of all time-points difference. (*B*) Difference of deuterium uptake (Da) between LCAT treated with IDFP (top) and without IDFP (bottom). Peptides with significant differences (stronger protection) are marked with the red bar along with their corresponding residue numbers.

Figure S8

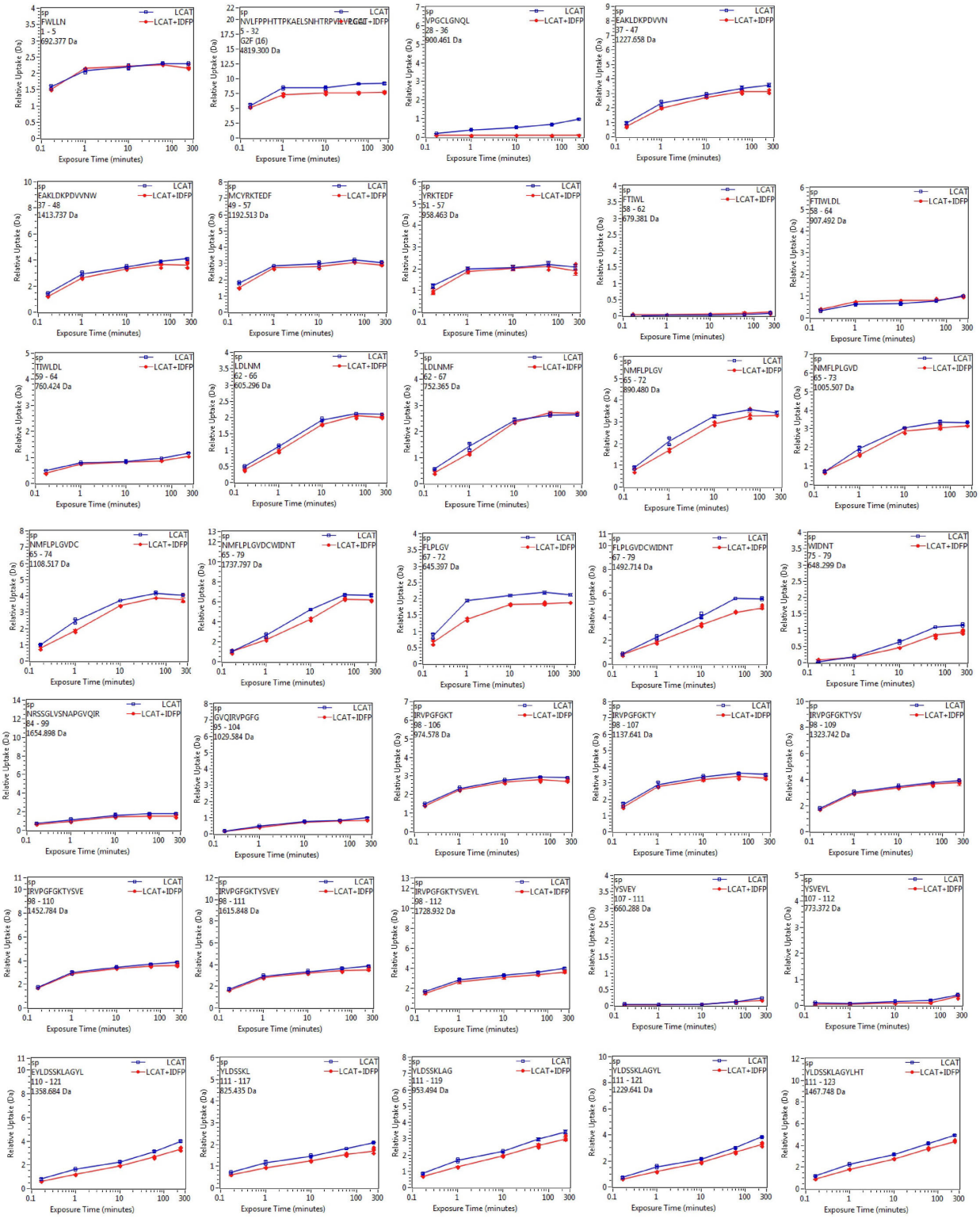
LCAT
LCAT+IDFP
Relative Uptake (Da)
Exposure Time (minutes)
sp
FWLLN
5 - 5
692.377 Da
sp
NVLFPPHTTPKAELSNHTRPVEGGT
5 - 32
G2F (16)
4819.300 Da
sp
VPGCLGNQL
28 - 36
900.461 Da
sp
EAKLDKPDVVN
37 - 47
1227.658 Da
sp
EAKLDKPDVVNW
37 - 48
1413.737 Da
sp
MCVRKTEDF
49 - 57
1192.513 Da
sp
VRKTEDF
51 - 57
958.463 Da
sp
FTIWL
58 - 62
679.381 Da
sp
FTIWLDL
58 - 64
907.492 Da
sp
TIWLDL
59 - 64
760.424 Da
sp
LDLNM
62 - 66
605.296 Da
sp
LDLNMF
62 - 67
752.365 Da
sp
NMFLPLGV
65 - 72
890.480 Da
sp
NMFLPLGVD
65 - 73
1005.507 Da
sp
NMFLPLGVDC
65 - 74
1108.517 Da
sp
NMFLPLGVDCWIDNT
65 - 79
1737.797 Da
sp
FLPLGV
67 - 72
645.397 Da
sp
FLPLGVDCWIDNT
67 - 79
1492.714 Da
sp
WIDNT
75 - 79
648.299 Da
sp
NRSSGLVSNAPGVQIR
84 - 99
1654.898 Da
sp
GVQIRVPGFG
95 - 104
1029.584 Da
sp
IRVPGFGKT
98 - 106
974.578 Da
sp
IRVPGFGKTY
98 - 107
1137.641 Da
sp
IRVPGFGKTYSV
98 - 109
1323.742 Da
sp
IRVPGFGKTYSVE
98 - 110
1452.784 Da
sp
IRVPGFGKTYSVEV
98 - 111
1615.848 Da
sp
IRVPGFGKTYSVEYL
98 - 112
1728.932 Da
sp
YSVEV
107 - 111
660.288 Da
sp
YSVEYL
107 - 112
773.372 Da
sp
EYLDSSKLAGYL
110 - 121
1358.684 Da
sp
YLDSSKL
111 - 117
825.435 Da
sp
YLDSSKLAG
111 - 119
953.494 Da
sp
YLDSSKLAGYL
111 - 121
1229.641 Da
sp
YLDSSKLAGYLHT
111 - 123
1467.748 Da

Figure S8 (continued)

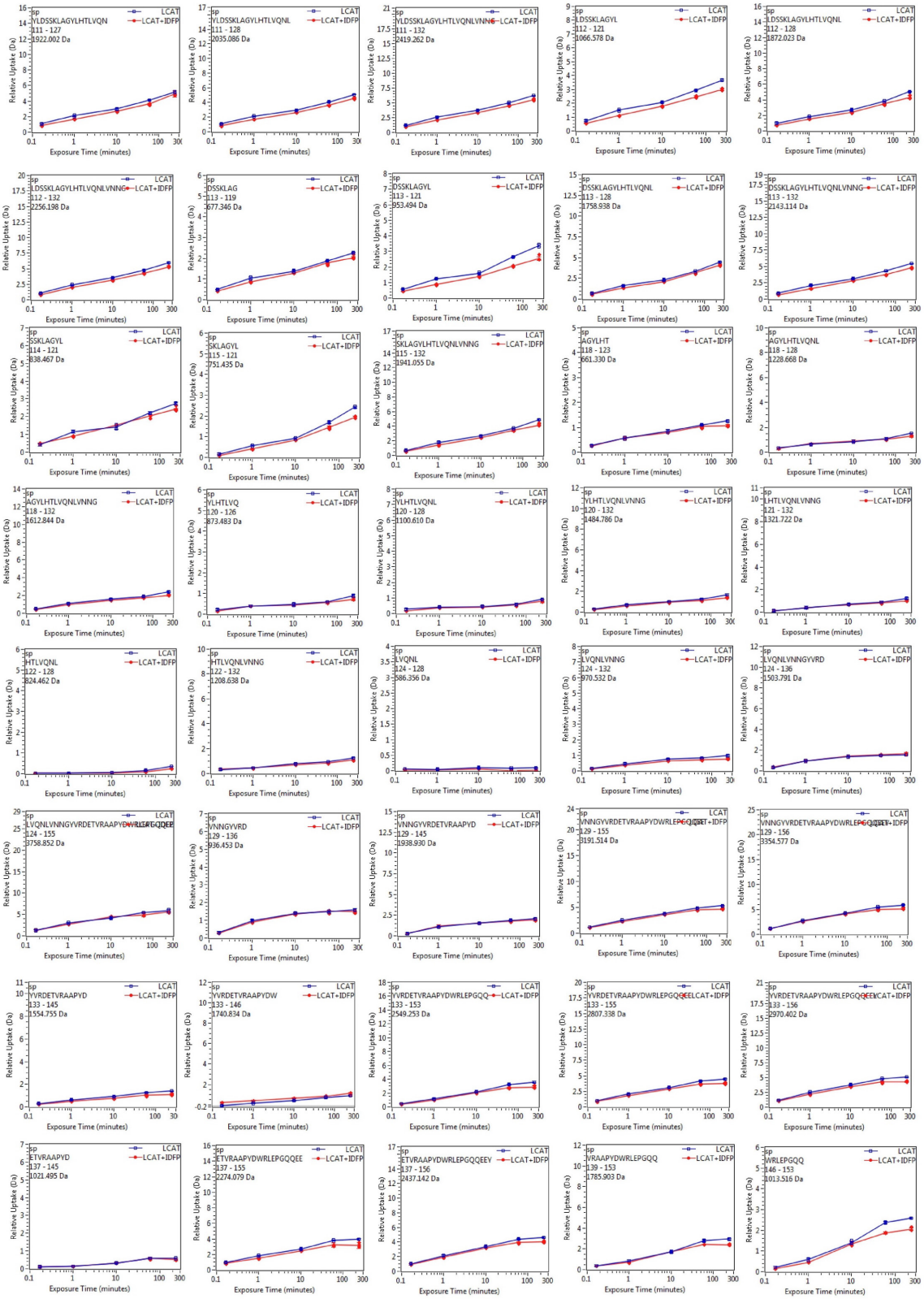

Figure S8 (continued)

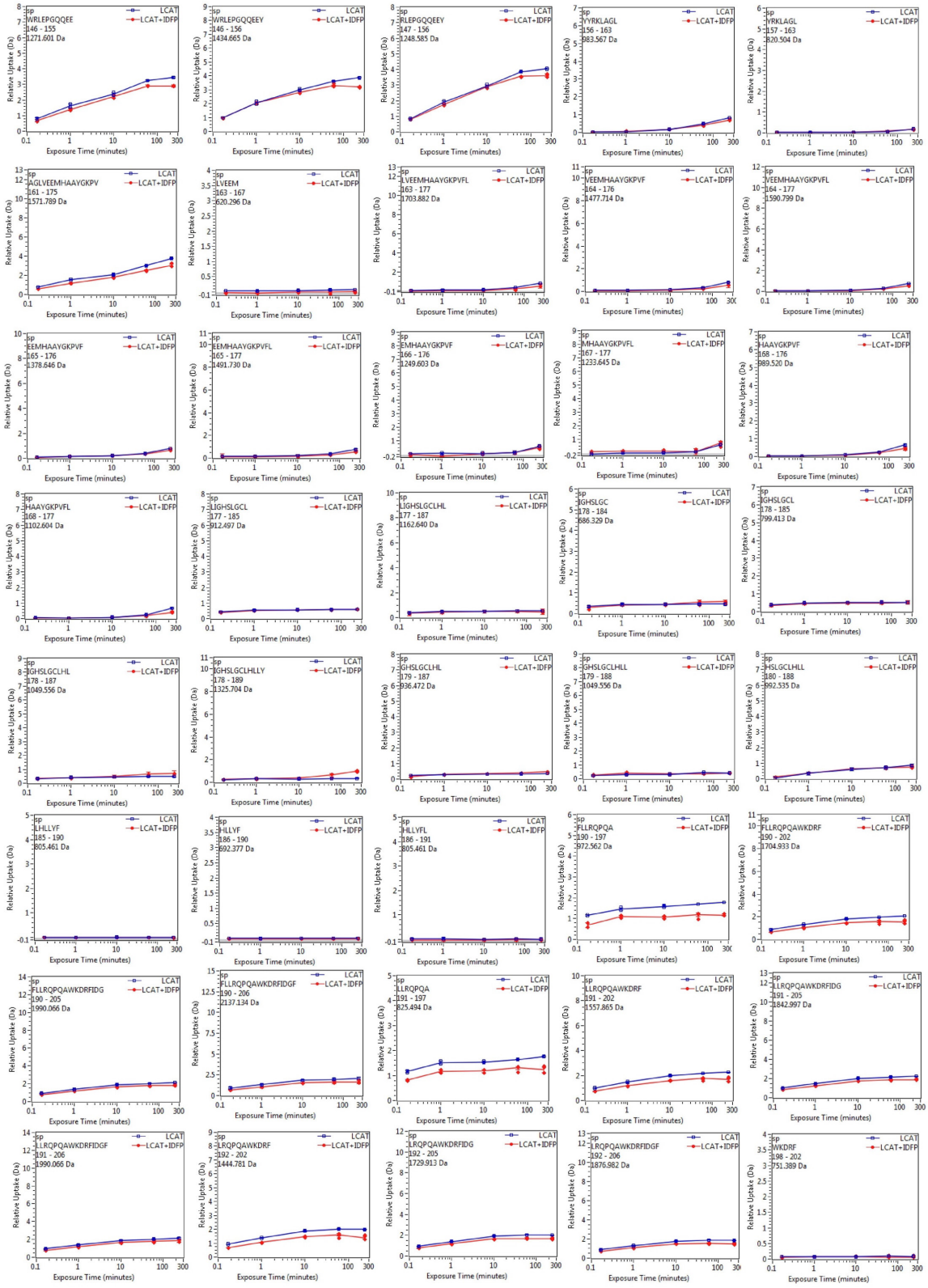

Figure S8 (continued)

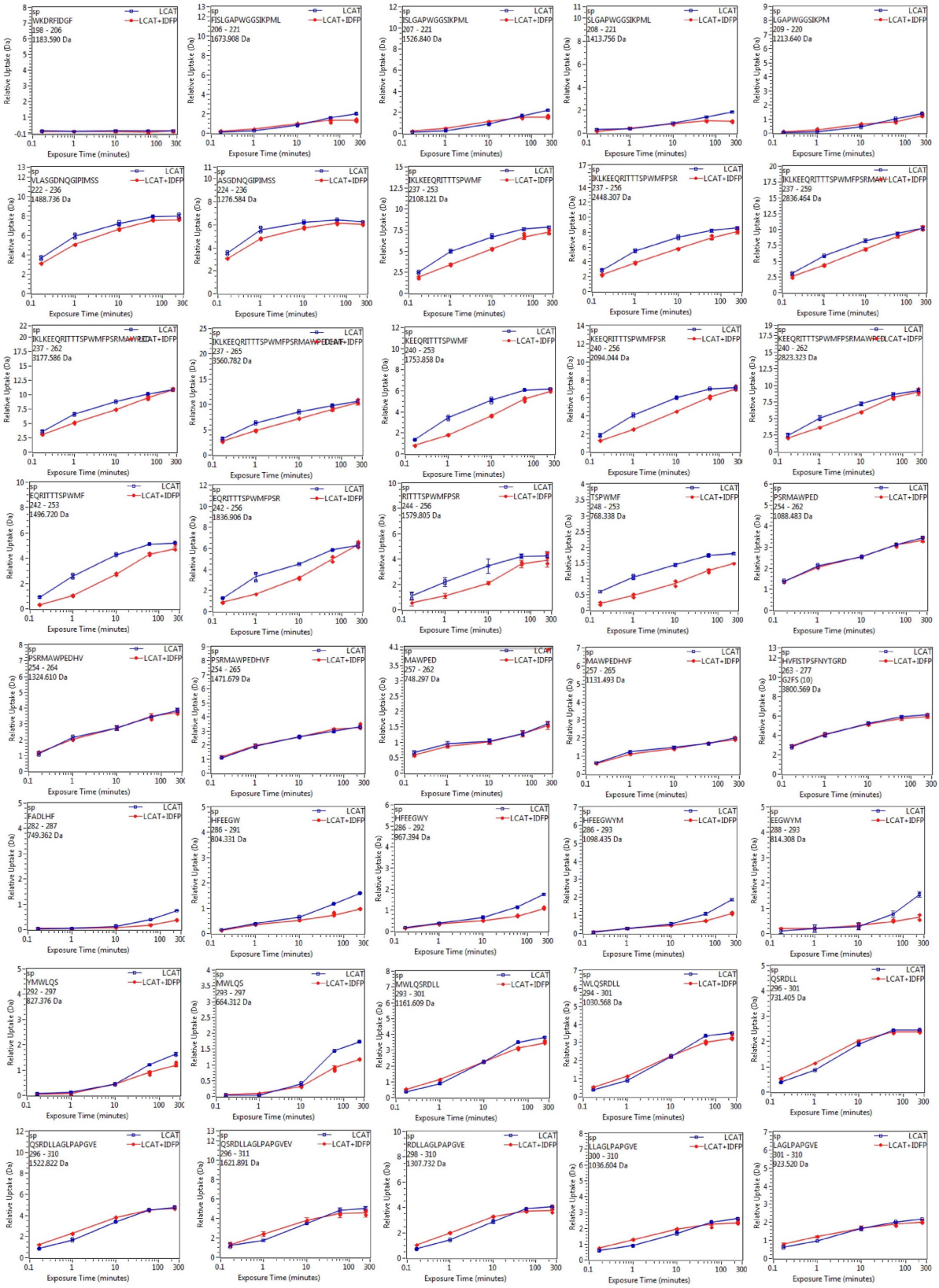

Figure S8 (continued)

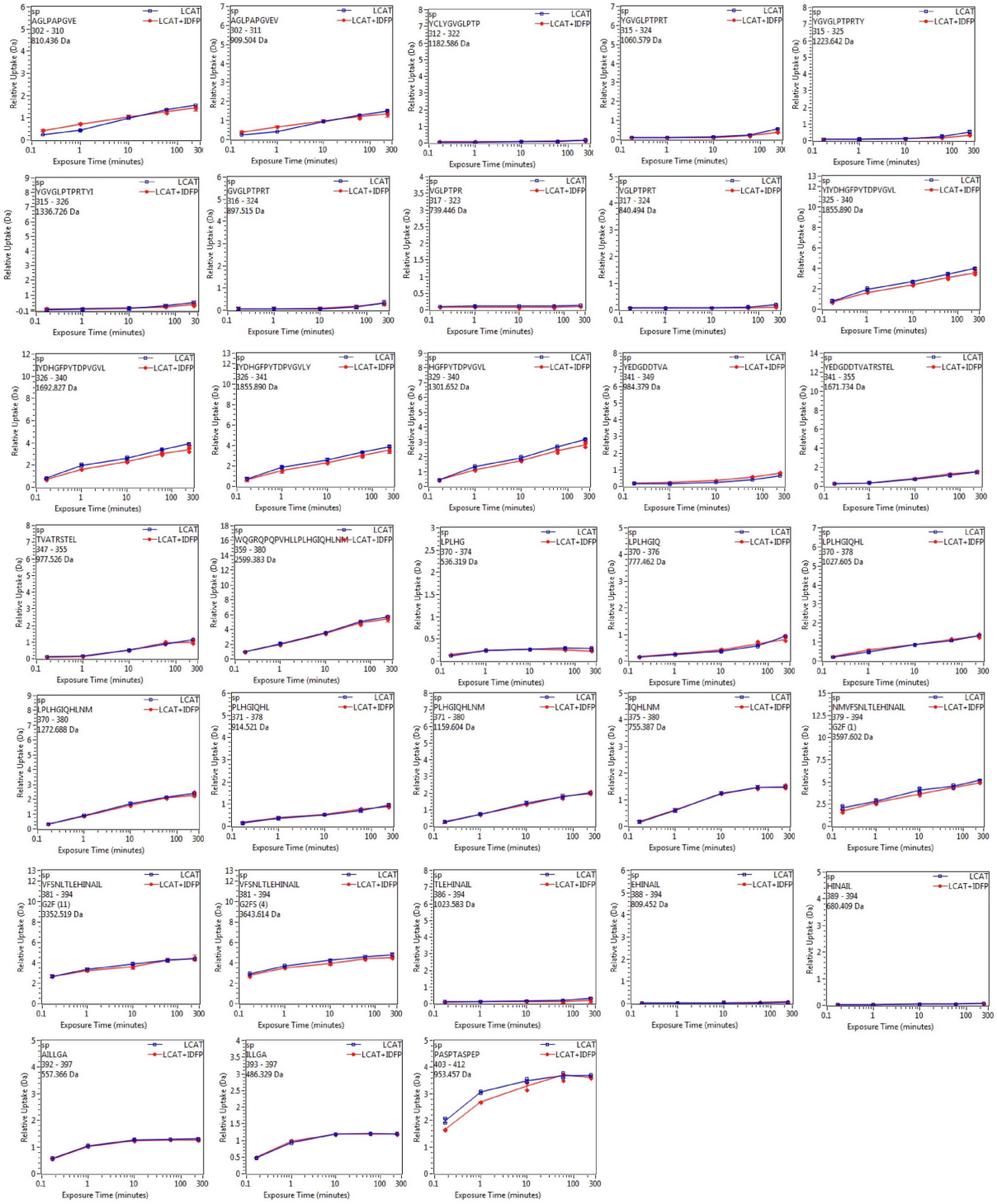

Figure S7. Deuterium uptake curves for a total of 187 peptides in the sequence coverage map. Native and IDFP-bound individual peptide deuterium uptake curves are compared at 5 time-points.

Figure S9

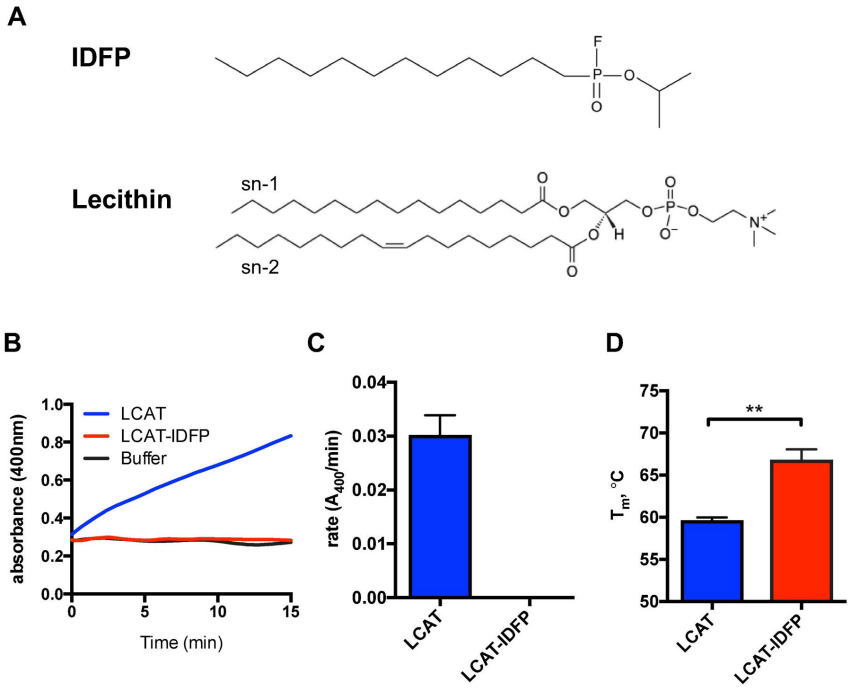

Figure S9. LCAT derivatization with IDFP. (*A*) Chemical structures of isopropyl dodecyl fluorophosphonate (IDFP) and lecithin. (*B*) pNPB esterase activity of IDFP-treated LCAT is compared to LCAT alone and buffer alone as a control. IDFP treated LCAT showed no activity on the soluble substrate pNPB, confirming that LCAT was fully derivatized. (*C*) The rate of esterase activity with error bars representing the standard deviation from three independent experiments. (*D*) DSF T_m values of LCAT with and without IDFP at 200 μM. Treatment with IDFP increased the T_m by 7 °C, indicating that IDFP-bound LCAT is more stable than LCAT alone. Data are from three independent experiments performed in triplicate. ** indicates that the data are statistically significant, p value = 0.0058 (paired t-test).

Figure S10

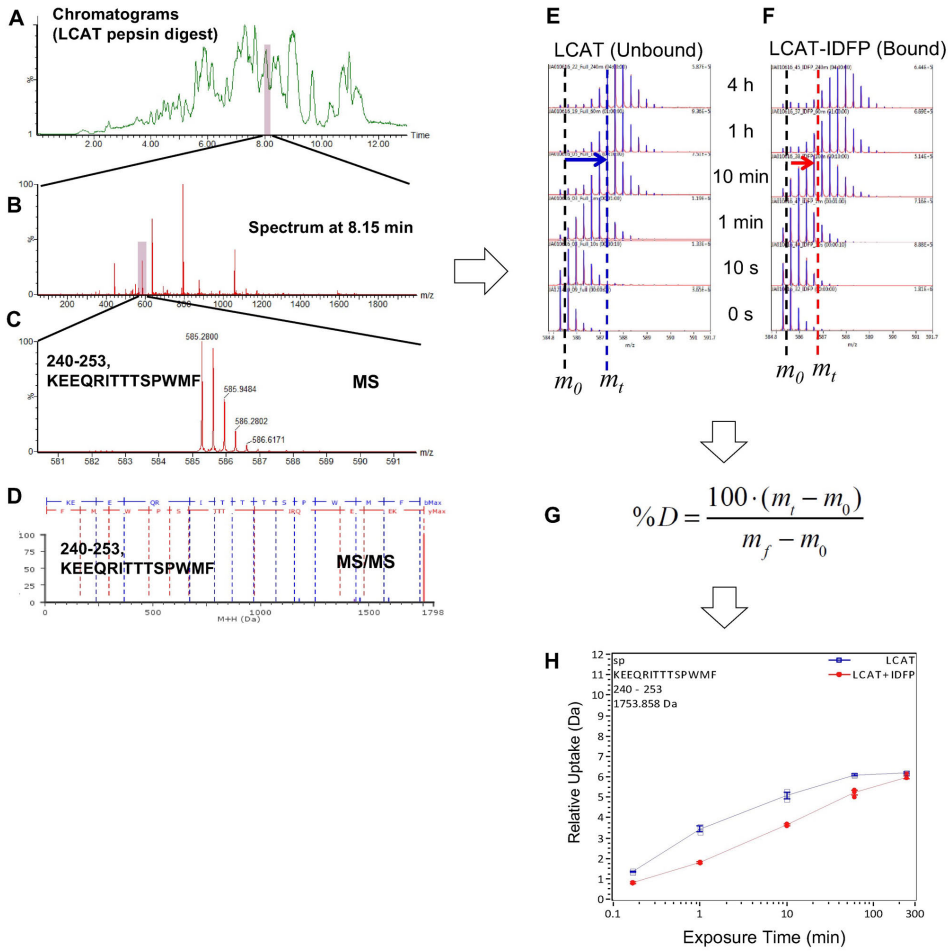

Figure S10. HDX MS data processing workflow. Representative chromatography of digested LCAT is shown in (*A*). The peptide KEEQRITTTSPWMF (240-253) is eluted at 8.15 min and its MS spectra are shown in (*B, C*) for undeuterated species. Its MS/MS spectrum with fragmentation ion identification is shown in (*D*). The time-course data at t = 0 s, 10 s, 1 min, 10 min, 60 min, and 240 min are processed (*E, F*) to determine the intensity weighted center mass (m_0 and m_t) and the normalized percent deuteration was determined using the equation in (*G*). The deuterium uptake of the selected peptide is plotted (*H*) for LCAT alone in blue and IDFP-bound LCAT in red.

Movie S1. Hypothetical transition between closed and open conformations of LCAT. The movie highlights the opening of the lid and corresponding cap domain movements that could occur upon HDL association. Thr123, Phe382, and the active site location Ser181 are shown as sticks. The closed and open–2Fab conformations of LCAT (PDB entries 5TXF and 5BV7, respectively) were aligned in PyMOL, and Chimera was used to morph from one structure to the other. The movie was rendered using PyMOL.